Mitochondrial fission in Huntington's disease mouse striatum disrupts ER-mitochondria contacts leading to disturbances in Ca^{2+} efflux and Reactive Oxygen Species (ROS) homeostasis

Marta Cherubini[a,b,c,1], Laura Lopez-Molina[a,b,c,1], Silvia Gines[a,b,c,*]

[a] *Departament de Biomedicina, Facultat de Medicina, Institut de Neurociències, Universitat de Barcelona, Barcelona, Spain*
[b] *Institut d'Investigacions Biomèdiques August Pi i Sunyer (IDIBAPS), Barcelona, Spain*
[c] *Centro de Investigación Biomédica en Red sobre Enfermedades Neurodegenerativas (CIBERNED), Madrid, Spain*

ARTICLE INFO

ABSTRACT

Mitochondria-associated membranes (MAMs) are dynamic structures that communicate endoplasmic reticulum (ER) and mitochondria allowing calcium transfer between these two organelles. Since calcium dysregulation is an important hallmark of several neurodegenerative diseases, disruption of MAMs has been speculated to contribute to pathological features associated with these neurodegenerative processes. In Huntington's disease (HD), mutant huntingtin induces the selective loss of medium spiny neurons within the striatum. The cause of this specific susceptibility remain unclear. However, defects on mitochondrial dynamics and bioenergetics have been proposed as critical contributors, causing accumulation of fragmented mitochondria and subsequent Ca^{2+} homeostasis alterations. In the present work, we show that aberrant Drp1-mediated mitochondrial fragmentation within the striatum of HD mutant mice, forces mitochondria to place far away from the ER disrupting the ER-mitochondria association and therefore causing drawbacks in Ca^{2+} efflux and an excessive production of mitochondria superoxide species. Accordingly, inhibition of Drp1 activity by Mdivi-1 treatment restored ER-mitochondria contacts, mitochondria dysfunction and Ca^{2+} homeostasis.

In sum, our results give new insight on how defects on mitochondria dynamics may contribute to striatal vulnerability in HD and highlights MAMs dysfunction as an important factor involved in HD striatal pathology.

1. Introduction

Mitochondria are dynamic organelles that provide energy to cells and buffer intracellular calcium (Ca^{2+}). In neurons, which critically depend on mitochondria function due to their high-energy demands, mitochondria can travel from the soma to dendritic and axonal processes to supply local necessities of Adenosine triphosphate (ATP) and Ca^{2+} maintenance. To ensure a proper distribution, mitochondria dynamically undergo shape changes modulated through regulated fission and fusion events (Frederick and Shaw, 2007; Campello and Scorrano, 2010).

Mitochondria are not isolated structures but interact with other organelles. The best characterized inter-organelle crosstalk is between mitochondria and endoplasmic reticulum (ER). These contact sites called *mitochondria-associated membranes* (MAMs) are specialized regions that act as a signaling hub to regulate cellular Ca^{2+} homeostasis (Rusiñol et al., 1994; Rizzuto et al., 1998; Csordás et al., 2006). Indeed, it has been reported that ER releases calcium in this specialized membrane hotspots directed towards mitochondria in order to maintain cellular bioenergetics and mitochondrial dynamics and therefore, cellular lifespan (Szabadkai et al., 2006; Rowland and Voeltz, 2012). These contact sites are characterized by a proteome enriched in

proteins involved in MAMs function. Thus, the Ca^{2+} channel inositol-1,4,5-triphosphate (IP3) receptor (IP3R) in the ER associates with the protein voltage-dependent anion channel isoform 1 (VDAC1) in the outer mitochondrial membrane. This interaction is strengthened through the molecular chaperone glucose-regulated protein 75 (GRP75) and the mitochondrial protein mitofusin-2 (Mfn2) allowing an efficient efflux of Ca^{2+} (Szabadkai et al., 2006; De Brito and Scorrano, 2008; Mendes et al., 2005). In this scenario, it is not surprising that either upregulation or disruption of ER-mitochondria contacts will be predicted of neuronal dysfunction and cell death distinctive of several neurodegenerative disorders (Calì et al., 2013a). Indeed, alterations in MAMs-related proteins have been reported in Alzheimer's disease (Area-Gomez et al., 2012; Hedskog et al., 2013), Parkinson's disease (Calì et al., 2013b; Ottolini et al., 2013) and Amyotrophic lateral sclerosis (Stoica et al., 2014). However, no evidence of ER-mitochondria contact alterations have been demonstrated in Huntington's diseases (HD). HD is an autosomal dominant neurodegenerative disorder characterized by a classic triad of symptoms consistent on movement disorders, psychiatric disturbances and cognitive decline (Huntington, 1872; Ross and Margolis, 2001). Mutant huntingtin (mHtt) causes the preferential degeneration of medium spiny neurons within the striatum (Vonsattel et al., 1985) that expands to other brain regions throughout the disease (Vonsattel and DiFiglia, 1998). The mechanism of this selective neuronal dysfunction and death remains elusive. Though several pathologic processes have been proposed, strong evidence from studies in humans and animal models suggests the involvement of mitochondrial dysfunction (Panov et al., 2002; Orr et al., 2008). Thus, indicators of mitochondrial defects including decreased ATP and free radical production, respiratory complex inhibition, loss of mitochondrial membrane potential and Ca^{2+} buffering disturbances have been recognized in HD (Giacomello et al., 2011; Reddy, 2014). In this line, previous studies from our group and others have demonstrated that mitochondrial fusion and fission are significantly perturbed and imbalanced in HD leading to accumulation of fragmented and damaged mitochondria with the subsequent increase in oxidative stress and energy defects (Cherubini et al., 2015; Shirendeb et al., 2011; Song et al., 2011). Though the precise mechanisms underlying excessive mitochondrial fragmentation in HD are not clear, it has been suggested that mHtt could induce Drp1 activity by direct interaction (Song et al., 2011; Shirendeb et al., 2012) or modulation of Drp1 S-nitrosylation levels (Nakamura et al., 2013). Accordingly, mutant huntingtin-induced-mitochondria and synaptic damage can be prevented by pharmacological inhibition of Drp1 activity by Mdivi-1 (Manczak and Hemachandra Reddy, 2015).

With all these evidences, in this work, we sought to analyze whether proneness of HD striatal mitochondria to undergo fragmentation could result in loss of ER-mitochondria contacts, and therefore, disruption of the correct Ca^{2+} buffering by the mitochondria. We postulate that this disruption, would contribute to Ca^{2+} dyshomeostasis increasing HD striatal vulnerability.

2. Materials and methods

2.1. Mice

R6/1 heterozygous transgenic mice (B6CBA background) expressing the exon-1 of mhtt with 145 CAG repeats. Our R6/1 mice colony expresses 145 CAG repeats instead of 115 CAG repeats of the original R6/1 mice due to CAG repeat instability as has been previously described by other groups (Morton et al., 2009; Møllersen et al., 2010). Heterozygous mutant $Hdh^{Q7/Q111}$ knock-in mutant mice, with targeted insertion of 109 CAG repeats that extends the glutamine segment in murine huntingtin to 111 residues and wild type $Hdh^{Q7/Q7}$ mice, were maintained on a C57BL/6 genetic background. Female $Hdh^{Q7/Q7}$ mice were crossed with male $Hdh^{Q7/Q111}$ mice to generate age-matched $Hdh^{Q7/Q7}$ wild type (WT) and $Hdh^{Q7/Q111}$ ($Hdh^{+/Q111}$) littermates, determined by

Polymerase Chain Reaction (PCR) analysis. Mice were housed with access to food and water ad libitum in a colony room kept at 19–22 °C, under a 12:12 h light/dark cycle. All mice used in the present study were males and were housed together in numerical birth order in groups of mixed genotypes. All procedures involving animals were performed in compliance with the National Institutes of Health Guide for the Care and Use of Laboratory Animals, and approved by the local animal care committee of the Universitat de Barcelona (99/01) and Generalitat de Catalunya (99/1094), in accordance with the European (2010/63/EU) and Spanish (RD53/2013) regulations for the care and use of laboratory animals.

2.2. Primary neuronal cultures

Dissociated striatal, cortical and hippocampal primary cultures prepared from E17.5 wild type (WT) and R6/1 embryos were plated at a density of 40,000 or 80,000 neurons for immunocytochemistry and transfections respectively, onto 12 mm coverslips placed in 24-well plates or at a density of 80–90,000 neurons onto 25 mm coverslips pre-coated with 0.1 mg/ml poly-D-lysine (Sigma Chemical Co., St. Louis, MO) placed in 6-well plates for calcium analysis. Neurons were cultured in Neurobasal medium (Gibco-BRL, Renfrewshire, Scotland, UK) supplemented with Glutamax and B27 (Gibco-BRL). Cultures were maintained at 37 °C in a humidified atmosphere containing 5% CO2. All experiments with neuronal cultures were analyzed 14 days after plating (DIV 14).

2.3. Plasmids and cell transfection

Fluorescent labelling of mitochondria and endoplasmic reticulum was achieved transfecting primary striatal neurons with pDsRed2-Mito and GFP-Sec61-β constructs, respectively. The pDsRed2-Mito vector (Clontech Laboratories; no. 632421) encodes a fusion of *Discosoma* sp. red fluorescent protein (DsRed2) and a mitochondrial targeting sequence of human cytochrome *c* oxidase subunit VIII (Mito). The GFP-Sec61-β vector, expressing the ER membrane protein Sec61β tagged with the green-fluorescent protein (GFP), was kindly supplied by Dr. Rapoport through the Addgene platform (Addgene; no. 15108). Primary neurons were transfected with Neuromag as instructed by the manufacturer (OZ Biosciences, France). Striatal primary neurons were transfected with 1 μg of both plasmids at DIV 10, fixed with 4% PFA/phosphate buffer and then analyzed at DIV 14.

2.4. Drug treatment

To assess the effect of dynamin-related protein 1 (Drp1) inhibition on mitochondrial dynamics and function, primary striatal neurons at DIV 14, were exposed to 25 μM of Mitochondrial division inhibitor 1 (Mdivi-1; Sigma Chemical Co., St. Louis, MO) for 1 h. Vehicle group was treated with 25 μM of dimethyl sulfoxide (DMSO). After treatment, cells were fixed with 4% paraformaldehyde (PFA)/phosphate buffer for immunocytochemistry analysis or prepared for calcium measurement assays.

2.5. Immunocytochemistry

For immunocytochemistry analysis, neurons were fixed at DIV 14 with 4% PFA/phosphate buffer for 10 min, rinsed in phosphate buffered saline (PBS), blocked in PBS containing 0.1 M glycine for 10 min, permeabilized in PBS containing 0.1% saponin for 10 min and finally blocked in PBS containing Normal Horse Serum 15% for 30 min at room temperature. Neurons were then washed in PBS and incubated overnight at 4 °C with primary antibody Microtubule-associated protein 2 (MAP2) (1:500, Sigma-Aldrich) or TOM-20 (1:250, ProteinTech) and detected with AlexaFluo488 anti-mouse (1:100, Jackson InmunoResearch), AlexaFluo488 anti-rabbit (1:100, Jackson

InmunoResearch), Cy3 anti-rabbit (1:100, Jacson InmunoResearch) or Cy3 anti-mouse (1:100, Jacson InmunoResearch).

2.6. Confocal images acquisition

Immunofluorescence was analyzed by confocal microscopy using a Leica TCS SP5 laser scanning confocal microscope (Leica Microsystems CMS GmbH, Germany). Images were taken using a HCX PL APO lambda blue 63.0×1.40 OIL objective with a standard pinhole (1 AU). For each image, z-stacks were taken from the entire three-dimensional structure. Digital zoom and size of stack depended on the experiment.

2.7. Analysis of mitochondria morphology

Mitochondrial morphology was analyzed as previously described (Cherubini et al., 2015; Koopman et al., 2006). Briefly, for quantitative analysis, digital images with 3.0 digital zoom and stacks of 0.4 μm were processed through a convolve filter and automatically thresholded using ImageJ software. From binary image, individual mitochondria were subjected to particle analyses to obtain number of mitochondria per cell, Aspect Ratio (AR, length-to-width ratio), and Form Factor (FF, ($Pm^2/4 \pi \times Am$), where Pm is the perimeter and Am is the surface area of mitochondrion. AR values of 1 mean a perfect circle, and the higher AR, the more elongated mitochondria. FF values of 1 indicate un-branched mitochondrion, and higher FF correspond to more complex mitochondria network. For each condition, 10–15 neurons were analyzed from 6 to 8 independent experiments.

2.8. ER-mitochondria co-localization analysis

For endoplasmic reticulum (ER)-mitochondria contact sites analysis, digital images were taking with 4.0 digital zoom and stacks of 0.2 μm. Stacks were automatically thresholded, deconvolved and the background was subtracted using ImageJ software. Interactions between organelles were quantified through Mander's co-localization coefficients obtained from ImageJ plugin "JACop". For each condition, 10–15 neurons were analyzed from 5 to 9 independent experiments.

2.9. Analysis of ER-mitochondria contacts by proximity ligation assay (PLA)

Proximity ligation assay (PLA) was performed using Duolink® detection kit with red fluorophore λ excitation 594 nm/λ emission 624 nm. After fixation and blocking, cells were first incubated with MAP2 (1:500, Sigma-Aldrich) to stain neurites in striatal neurons and then with primary antibodies IP3R3 (1:500, Merck, Germany) and VDAC1 (1:500, Abcam, UK) overnight. After washing with PBS, PLA probes anti-mouse PLUS and anti-rabbit MINUS were added for 1 h and hybridization was amplified by rolling circle amplification. Nuclei were stained with 4 '6-diamidino-2-fenilindol (DAPI) using mounting media provided in the kit. Digital images were taking with 3.0 digital zoom and stacks of 0.4 μm. Fluorescent dots were analyzed using the plugin "Analyze particles" of ImageJ. Number of particles were relativized to MAP2 area of interest. As a negative control, one of the primary antibodies was omitted.

2.10. Mitochondrial superoxide production

To evaluate mitochondrial superoxide production in cultures, striatal primary neurons at DIV 14 were incubated with MitoSOX™ Red Indicator (Molecular Probes, Invitrogen) for 30 min at 37 °C. Cells were then fixed with 4% PFA/phosphate buffer and nuclei stained with DAPI. Digital images with 4.0 digital zoom and stacks of 0.4 μm were processed through a convolve filter, background was subtracted and automatically thresholded using ImageJ software. MitoSOX intensity was calculated as Integrated Density/Area of cell. For each condition, 15

neurons were analyzed from 7 to 8 independent experiments.

2.11. Western blot analysis

Animals were sacrificed by cervical dislocation and striatum, hippocampus, and cortex were dissected. Tissue was homogenized by sonication in lysis buffer (50 mM Tris base, pH 7.5, 10 mM EGTA, 150 mM NaCl, protease inhibitor mixture and 1 mM sodium orthovanadate) and centrifuged at $10,000 \times g$ for 10 min. Supernatant was collected and protein content was measured by Detergent-Compatible Protein Assay (Bio-Rad, Hercules, CA, USA). Protein extracts (20 μg) were denatured in 62.5 mM Tris-HCl (pH 6.8) 2% SDS, 10% glycerol, 140 mM β-mercaptoethanol and boiled for 5 min. Protein samples were resolved on 6–10% SDS-PAGE and transferred onto nitrocellulose membranes. Blots were blocked with 10% non-fat powdered milk in Tris-buffered saline Tween-20 (TBS-T) for 1 h at room temperature. Membranes were incubated overnight at 4 °C with primary antibodies: Drp1 (DLP1; 1:1000; BD Bioscience), Grp75 (1:2000, Abcam), IP3R3 (1:500, BD), Mfn2 (1:2000, Abcam), Calnexin (1:1000, Santa Cruz), Calreticulin (1:1000, Santa Cruz), Nogo (1:1000, Santa Cruz), and Stim1 (1:1000, Santa Cruz). For protein loading control, membranes were incubated 20 min with an antibody against α-tubulin (1:50,000, Sigma Aldrich). After primary antibody incubation, membranes were rinsed three times for 10 min with TBS-T and incubated for 1 h at room temperature with a horseradish peroxidase-conjugated secondary antibody (1:3000, Promega). Inmunoreactive bands were visualized using ECL kit (Santa Cruz) and quantified by using Image J software.

2.12. Calcium measurement

To detect cytosolic Ca^{2+} changes (Cai^{2+}), wild type and R6/1 primary striatal neurons, cultured on glass coverslips during 14 days (DIV 14), were washed with Krebs buffer (145 mM NaCl, 5 mM KCl, 10 mM HEPES, 1 mM MgCl$_2$, 1 mM CaCl$_2$, 5.6 mM glucose and pH 7.4/NaOH) and loaded with 5 μm Fluo-4 AM/0.02% Pluronic F-127 (Molecular Probes, Invitrogen) at room temperature in the dark for 30 min. After rinsing with fresh buffer, cells were loaded with 20 nM tetramethylrhodamine methyl ester (TMRM; Molecular Probes, Invitrogen) at room temperature in the dark for 20 min in order to detect changes in mitochondrial membrane potential (ΔΨm). Cells were then washed and coverslips were assembled in a chamber filled with 500 μl of buffer containing TMRM on the stage of the Leica confocal microscope equipped with an incubation system with temperature and CO$_2$ control. After a 5 min equilibration time, neurons were exposed to 0.5 μM Thapsigargin (TG; Sigma-Aldrich), a SERCA ATPase inhibitor that increases the concentration of intracellular Ca^{2+} by blocking its storage in the ER. Simultaneously, TMRM was excited at 543 nm and the emission collected with a 560 nm long-pass filter, and Fluo-4 was excited at 488 nm and the emission collected through a 505–550 nm barrier filter. Experiments were terminated inducing a maximal mitochondrial depolarization by addition of 2 μM Carbonyl cyanide 4-(trifluoromethoxy) phenylhydrazone (FCCP; Sigma-Aldrich), an uncoupler of respiratory chain oxidative phosphorylation that depolarizes mitochondrial membrane determining Ca^{2+} release into the cytosol. Images were captured every 2 s throughout about 8–10 min of experiment. The quantification of fluorescence intensities was calculated using ImageJ software and the values were normalized to the baseline images. Fluo 4 and TMRM fluorescence changes are showed as fold change of normalized response F/F0 where F0 is the fluorescence intensity at time zero; F is the corrected fluorescence intensity at a given time point.

2.13. Subcellular fractionation

Microsomal fractions were obtained as described in Bozidis et al. (2007). Briefly, striata from three different mice (wild type or R6/1)
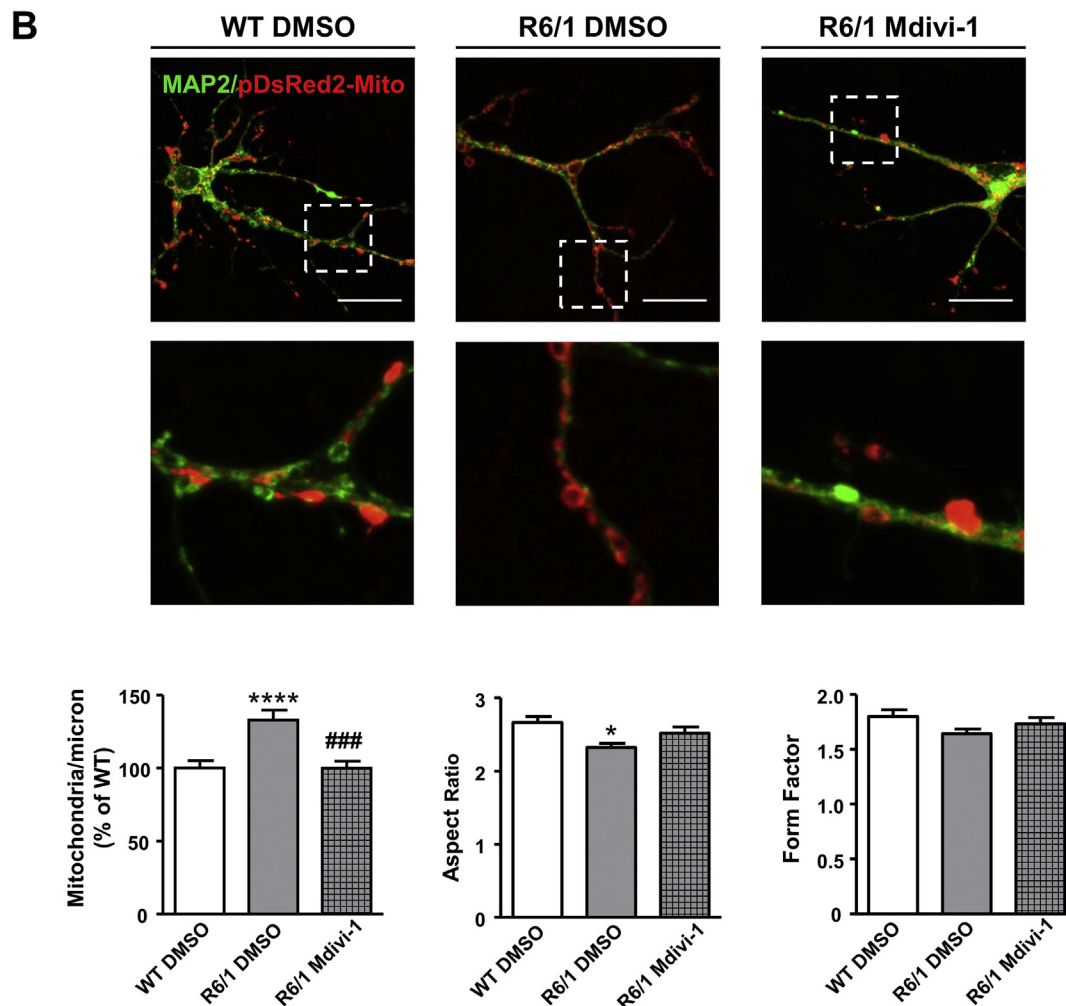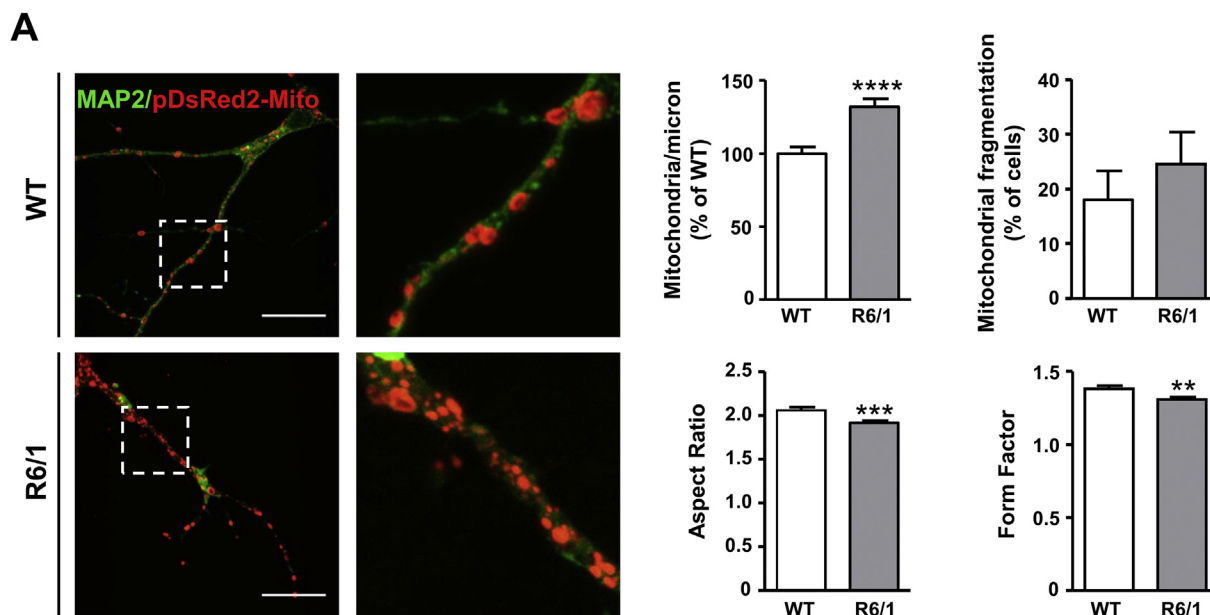
A

B

**Fig. S7.** Levels of MAM proteins IP3R3, Grp75 and Mfn2 are not altered in cortical and hippocampal HD postmortem brain samples. Representative Western blots showing Grp75, IP3R3 and Mfn2 levels in cortical and hippocampal extracts from control (n = 6) and HD postmortem brain samples (n = 8). α-tubulin was used as loading control. Histograms show relative protein levels expressed as percentage of controls.
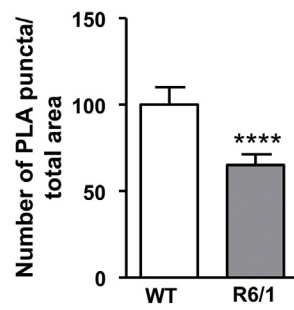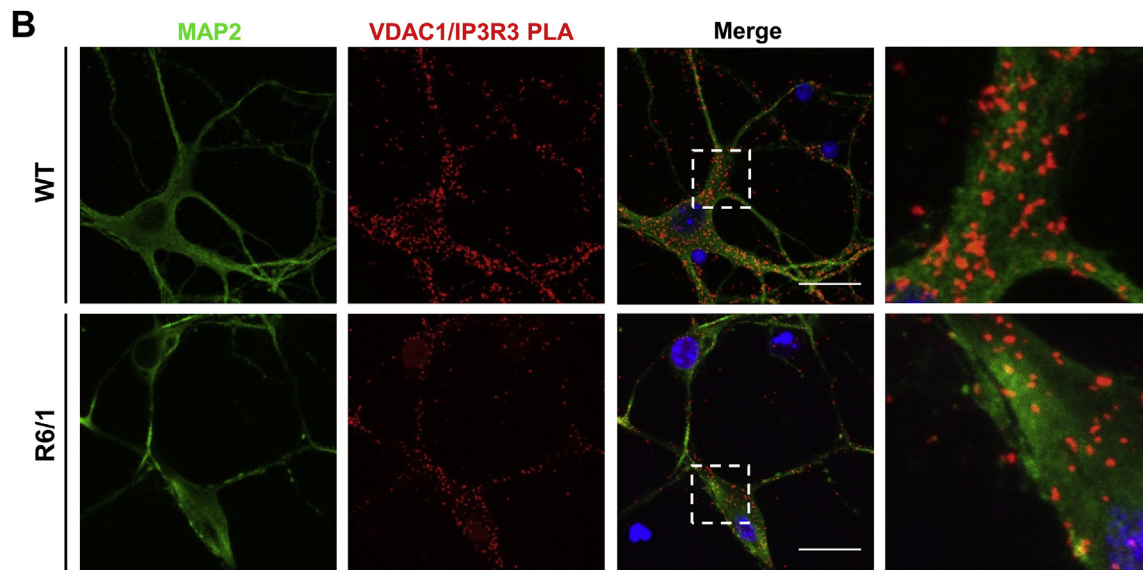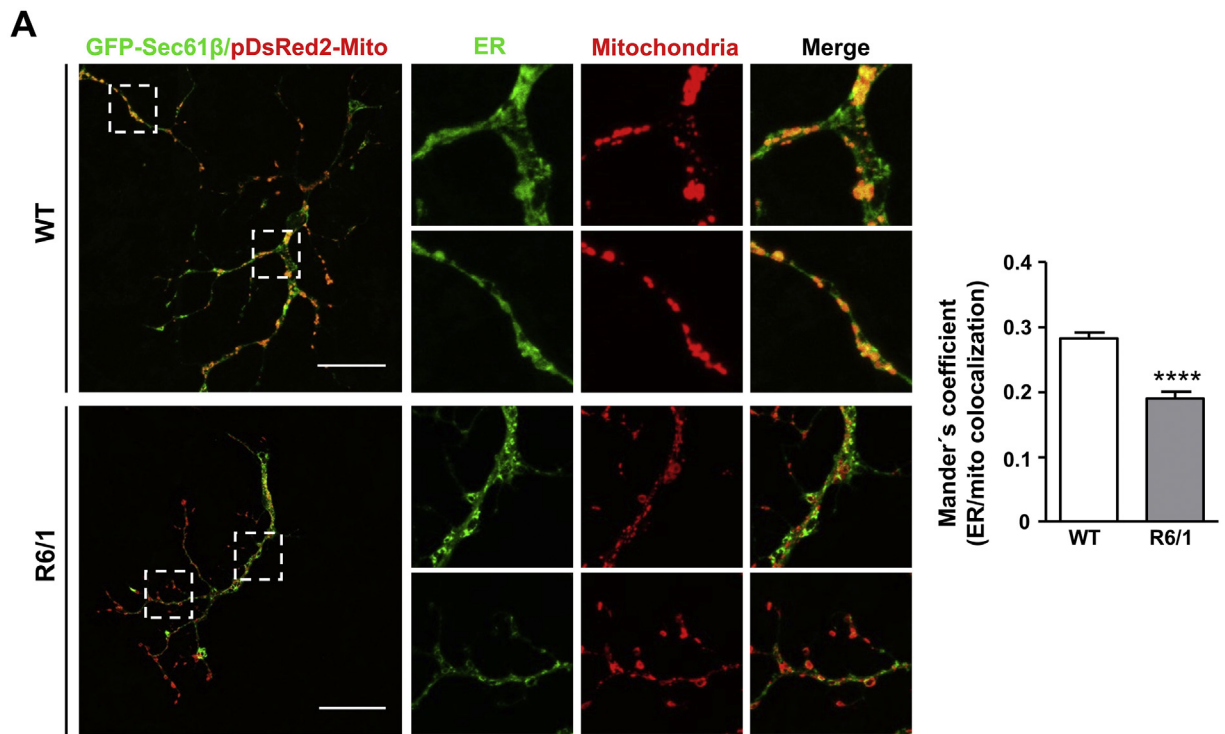
(caption on next page)

were pooled and homogenized with a dounce homogenizer in sucrose homogenization medium (0.25 M sucrose, 10 mM HEPES, pH 7.4). Samples were then centrifuged twice at 4 °C for 5 min at 600 $\times g$ and supernatant further centrifuged four times at 4 °C for 10 min at 10,300 $\times g$. The resultant supernatant was next ultracentrifuged at 4 °C for 60 min at 100,000 $\times g$ to pellet microsomes. Finally, the resultant microsomal fraction containing rough and smooth ER was resuspended in sucrose homogenization medium.

2.14. Statistical analysis

All the results were analyzed using GraphPad Prism software version 7.0. Data were presented as mean ± standard error of the means (SEM). Statistical analysis was performed using Student's *t*-test or Mann-Whitney test for two groups and Kruskal-Wallis followed by the post hoc Dunn's test for multiple comparison. Differences were considered statistically significant when *p* value < .05.

3. Results

3.1. Increased Drp1-dependent mitochondrial fragmentation in R6/1 striatal cultures

Excessive Drp1-mediated mitochondrial fission has been reported in R6/2 striatum as well as in other neuronal primary cultures overexpressing exon-1 with a HD polyQ expansion (Song et al., 2011; Guo et al., 2013). However, no data regarding mitochondrial morphology has been described in the striatum of R6/1 mice. Therefore, mitochondrial network was analyzed in striatal cultures from WT and R6/1 mice at DIV 14 transfected with pDsRed2-Mito and stained with MAP-2 for neurites (Fig. 1A). Morphometric analysis by confocal microscopy revealed higher mitochondrial fission in mutant R6/1 striatal cultures compared with WT cultures, as evidenced by a significant increase in the number of mitochondria within neuritic projections or a trend increase in the number of cells showing fragmented mitochondria (Fig. 1A). Accordingly, a significant reduction of mitochondrial length (Aspect Ratio; Fig. 1A) and mitochondrial complexity with decreased branching (Form Factor; Fig. 1A) was observed in mutant R6/1 striatal neurons. Notice the presence of donut-shape mitochondria in R6/1 striatal cultures likely related to mitochondrial oxidative stress (Ahmad et al., 2013). To assess whether changes in mitochondria dynamics were specific of the striatal brain area, mitochondria morphology was also evaluated in cortical (Fig. S1A) and hippocampal primary cultures (Fig. S1B). No significant differences between genotypes were found neither in cortical nor in hippocampal primary cultures, pointing the striatum as the most vulnerable region to mitochondria pathology in HD.

Drp1 increased activity has been proposed as a potential mechanism underlying mitochondrial fission in HD (Shirendeb et al., 2012; Costa et al., 2010). To test this possibility in our R6/1 striatal cultures, neuronal cells were incubated with Mdivi-1 (25 μM, 1 h), a well-known chemical inhibitor of the mitochondrial fission protein Drp1 (Cassidy-Stone et al., 2008) and mitochondrial network was analyzed (Fig. 1B). Treatment with Mdivi-1 was able to prevent mitochondrial fragmentation, showing R6/1 treated neurons values of mitochondria number, length and branching similar to those in WT vehicle cultures (Fig. 1B). According with these findings, Western blot analysis in R6/1 striatal primary cultures, demonstrated a trend increase in Drp1 tetrameric (~320 kDa) but not monomeric forms (~80 kDa) when compared with WT striatal cells (Fig. S2A). Notice that, Drp1 oligomerization has been associated, at least in part, with Drp1 activation (Guo et al., 2013; Cho et al., 2014; Zhu et al., 2004). Similarly, when Drp1 mRNA levels were evaluated a great increase, though not significant, in R6/1 versus WT striatal neuronal cells was found (Fig. S2B) All these findings demonstrate excessive mitochondrial fragmentation in R6/1 mutant striatal neurons that is dependent on Drp1 activity.

3.2. Diminished ER-mitochondria contact sites in R6/1 striatal cultures

Contacts between the ER and mitochondria at MAMs represent a critical intracellular signaling platform that regulates different and crucial cellular functions (Raturi and Simmen, 2013; Iwasawa et al., 2011). Given the increase in mitochondrial fission observed in R6/1 striatal cultures, we wondered whether disrupted mitochondrial network could also impair ER-mitochondria association. To this aim, WT and R6/1 striatal neurons (DIV 14) were transfected with GFP-Sec61β and pDsRed2-Mito to label ER and mitochondria respectively and co-localization studies were performed by using confocal microscopy (Fig. 2A). Analysis of immunofluorescence images revealed that a proportion of Sec61β overlapped with pDsRed2-Mito in both WT and R6/1 neurons, indicating ER-mitochondria association (Fig. 2A). However, co-localization levels were significantly lower in R6/1 striatal neurons compared with WT neurons as supported by the calculation of the Manders'colocalization coefficient, which suggest a significant decrease in ER-mitochondria contact sites in R6/1 (Fig. 2A). To further elaborate on these findings, we sought to use proximity ligation assays (PLA) to quantify the profusion of ER-mitochondria associations in WT and R6/1 striatal cultures (Fig. 2B). For these assays, we used VDAC1 and IP3R3 primary antibodies as probes for mitochondria and ER respectively, since these proteins are enriched at MAMs (Hedskog et al., 2013). MAP2 staining was used to determine neurite area and used to normalize PLA values. Negative controls showed no signal (Fig. S3A). Consistent with confocal analysis, the abundance of ER-mitochondria contact sites, measured as interaction between VDAC1 and IP3R3 (PLA puncta) was found to be lower in R6/1 compared to WT striatal neurons (Fig. 2B). Since reduced PLA signal can be due to lower expression of VDAC1 and/or IP3R3, we next determined the levels of both proteins in lysates from WT and R6/1 striatal cultures by Western blot analysis (Fig. S3B). No significant differences between genotypes were found either for VDAC1 or IP3R3, suggesting that reduced co-localization and interaction measured by confocal microscopy and PLA in R6/1 striatal cultures involve loss of ER-mitochondrial contacts.

3.3. Loss of ER-mitochondrial contacts can be reverted by preventing aberrant mitochondrial fission in R6/1 striatal cultures

Increased Drp1-mediated mitochondrial fission could be responsible of reducing ER-mitochondria contacts in R6/1 striatal neurons. To test this hypothesis, we analyzed in R6/1 neurons whether reversion of mitochondrial fragmentation by Mdivi-1 treatment was also accompanied by a rescue of ER-mitochondria tethers. As expected, R6/1 neurons showed fragmented mitochondria along with a significant decrease in ER-mitochondria contacts as supported by a lower Mander's co-localization coefficient (Fig. 3). Treatment with Mdivi-1 completely restored ER and mitochondria contacts, showing R6/1-treated neurons similar values to those found in WT neurons (Fig. 3). These findings indicate an important contribution of aberrant mitochondrial fragmentation to disrupted ER-mitochondrial contacts in R6/1 striatal cultured neurons.

3.4. Increased mitochondria superoxide production can also be reverted by inhibition of mitochondrial fission in R6/1 striatal cultures

Since mitochondrial function is dependent on their intact structure, we next analyzed in R6/1 striatal neurons whether Mdivi-1-mediated normalization of the mitochondrial network was also associated with a functional recovery of the mitochondria. To this aim, mitochondrial superoxide levels were determined by MitoSox Red staining (Fig. 4). A significant two-fold increase in mitochondrial superoxide levels was found in R6/1 compared to WT striatal neurons. Interestingly, inhibition of mitochondrial fission by treatment with Mdivi-1 returned mitochondrial superoxide to levels comparable to WT. These results suggest that disruption of mitochondria dynamics due to excessive

Fig. 1. R6/1 primary striatal neurons exhibit increased Drp1-dependent mitochondrial fragmentation. (A) Representative confocal images of striatal primary neurons from WT and R6/1 mice in basal conditions. Neurons were transfected with pDsRed2-mito in red and labelled with anti-MAP2 in green. Scale bar 20μm. The boxed areas are enlarged in the right panels. Bar histograms show the percentage of mitochondria per axonal micron, the percentage of cells with fragmented mitochondria, the relative Aspect Ratio and the relative Form Factor. Data represent mean ± SEM of 6-8 independent experiments with 10-15 neurons/genotype each. **p < 0.01, ***p < 0.001, ****p < 0.0001 vs WT as determined by unpaired Mann-Whitney test or Kruskal-Wallis test with Dunn's post hoc analysis. (B) Representative confocal images of striatal primary neurons from WT and R6/1 mice treated with vehicle (DMSO) or Mdivi-1 (25 μM). Bar histograms show the percentage of mitochondria per axonal micron, the relative Aspect Ratio and the relative Form Factor. Data represent mean ± SEM of 6-8 independent experiments with 10-15 neurons/genotype each. *p < 0.05, ****p < 0.0001 vs WT; ###p < 0.001 vs R6/1 DMSO as determined by unpaired Mann-Whitney test or Kruskal-Wallis test with Dunn's post hoc analysis (For interpretation of the references to colour in this figure legend, the reader is referred to the web version of this article.)
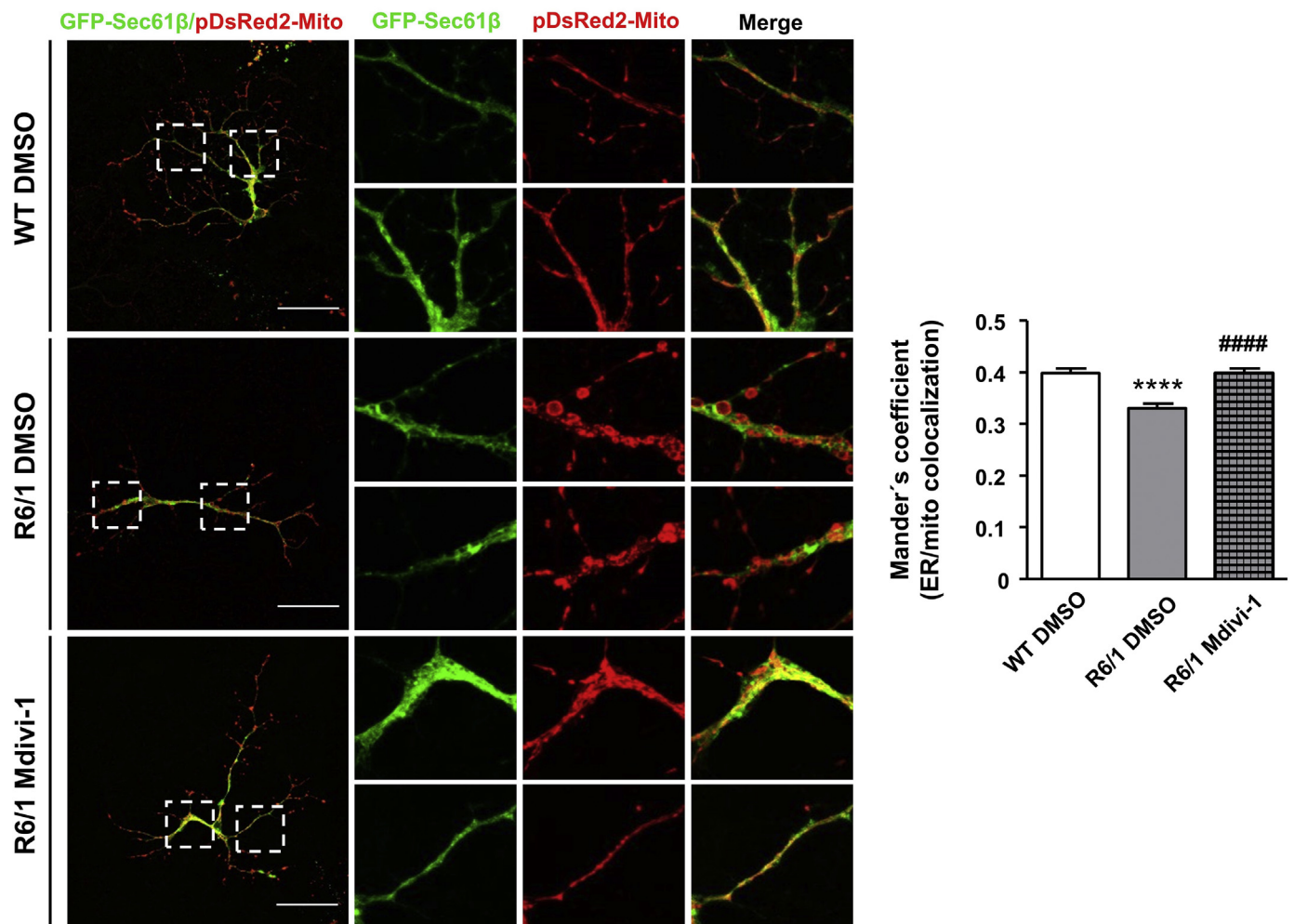

Fig. 2. ER-mitochondria contacts are diminished in R6/1 primary striatal neurons. (A) Representative confocal images of striatal primary neurons from WT and R6/1 mice transfected with GFP-Sec61-β in green and pDsRed2-mito in red. Scale bar 20 μm. Panels on the right show single and merged channels magnifications of the boxed areas. Bar histogram shows normalized Mander's coefficient values calculated from z-axis confocal stacks. Data represent mean ± SEM of 9 independent experiments with 10-15 neurons/genotype each. ****p < 0.0001 vs WT as determined by unpaired Mann-Whitney test. (B) Representative confocal images of VDAC1/IP3R3 interaction by in situ PLA in striatal primary neurons. Nuclei appear in blue, interactions between the two targeted proteins in red, and anti-MAP2 in green. Scale bar 20 μm. Bar histogram shows number of particles/total area. Data represent mean ± SEM of 8 independent experiments in which 20 neurons were examined per genotype using ImageJ software. **** p < 0.0001 as determined by unpaired Mann-Whitney test. (For interpretation of the references to colour in this figure legend, the reader is referred to the web version of this article.)

mitochondria fission likely impact on striatal oxidative stress status in R6/1 striatal neuronal cultures.

3.5. Specific reduction of MAMs proteins in the striatum of two different HD mice and in HD human brain

The contacts between ER and mitochondria (MAMs) depend on complementary membrane proteins that tether both organelles at specific sites (Rizzuto et al., 1998; Csordás et al., 2006). Even if no changes in some MAMs proteins have been found in R6/1 striatal cultures (Fig. S3B), we cannot discard deficiencies in MAMs protein expression in R6/1 brain tissue. Therefore, the expression of the glucose-regulated protein 75 (Grp75), the isoform 3 of the inositol triphosphate receptor (IP3R3), and mitofusin 2 (Mfn2), were determined in total lysates obtained from the striatum of WT and R6/1 mice at the age of 8, 12, 20 and 30 weeks by Western blot (Fig. 5A). To notice that at 12 weeks of age, R6/1 mice start to manifest motor coordination symptoms evaluated by the rotarod test (Anglada-Huguet et al., 2016). Compared with WT mice, a significant decrease in Grp75 levels was observed in R6/1 mice at 12 and 20 weeks of age, a reduction that was no evident at late disease stages (30 weeks). By contrast, when IP3R3 levels were analyzed, a significant decline was detected in R6/1 mice by 12 weeks of
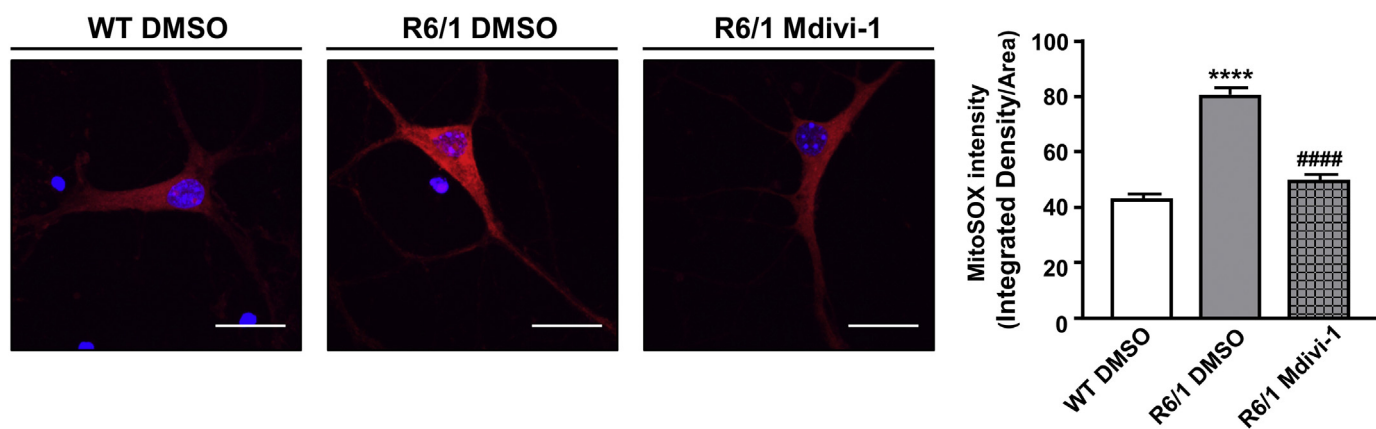
Fig. 3. Inhibition of mitochondria fission by Mdivi-1 recovers ER-mitochondria contact sites in R6/1 primary striatal neurons. Representative confocal images of striatal primary neurons from WT and R6/1 mice. Neurons were transfected with GFP-Sec61-β in green and pDsRed2-mito in red. Scale bar 50 μm. Panels on the right show single and merged channels magnifications of the boxed areas. Bar histogram shows normalized Mander's coefficient values calculated from z-axis confocal stacks. Data represent mean ± SEM of 5-6 independent experiments with 10 neurons/genotype each. ****p < 0.0001 vs WT; ####p < 0.0001 vs R6/1 DMSO as determined by unpaired Mann-Whitney test or Kruskal-Wallis test with Dunn's post hoc analysis. (For interpretation of the references to colour in this figure legend, the reader is referred to the web version of this article.)
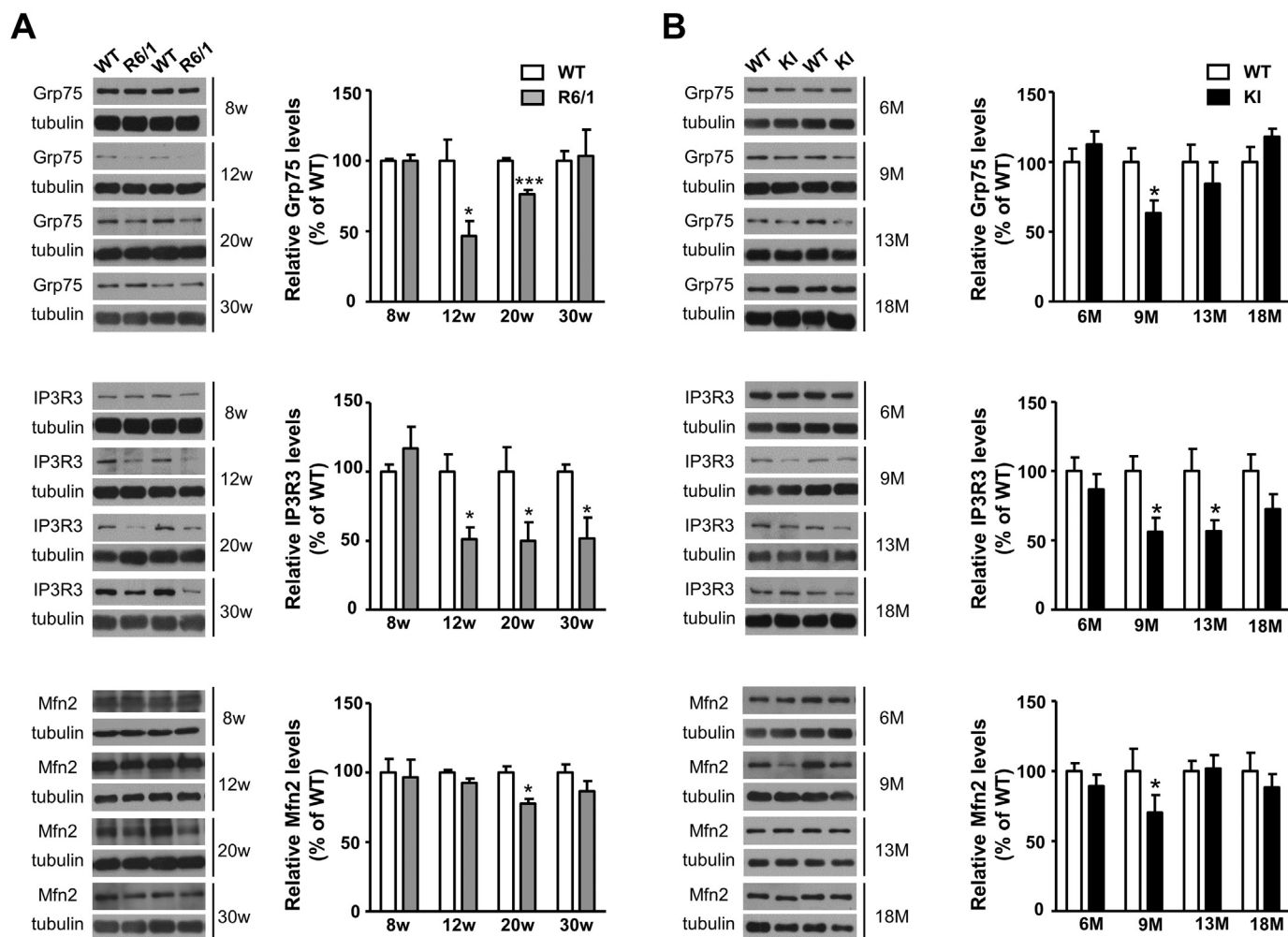
Fig. 4. Excessive mitochondrial superoxide production in R6/1 striatal primary neurons is normalized after Mdivi-1 treatment. Representative confocal images of striatal primary neurons from WT and R6/1 mice treated with vehicle (DMSO) or Mdivi-1 (25 μM). Mitochondrial superoxide production was determined using MitoSOX Red Indicator. Nuclei appear in blue. Scale bar 20 μm. Bar histogram shows intensity of MitoSOX per cell area. Data represent mean ± SEM of 7-8 independent experiments with 15 neurons/genotype each. ****p < 0.0001 vs WT, ####p < 0.0001 vs R6/1 DMSO as determined by Kruskal-Wallis test with Dunn's post hoc analysis (For interpretation of the references to colour in this figure legend, the reader is referred to the web version of this article.)
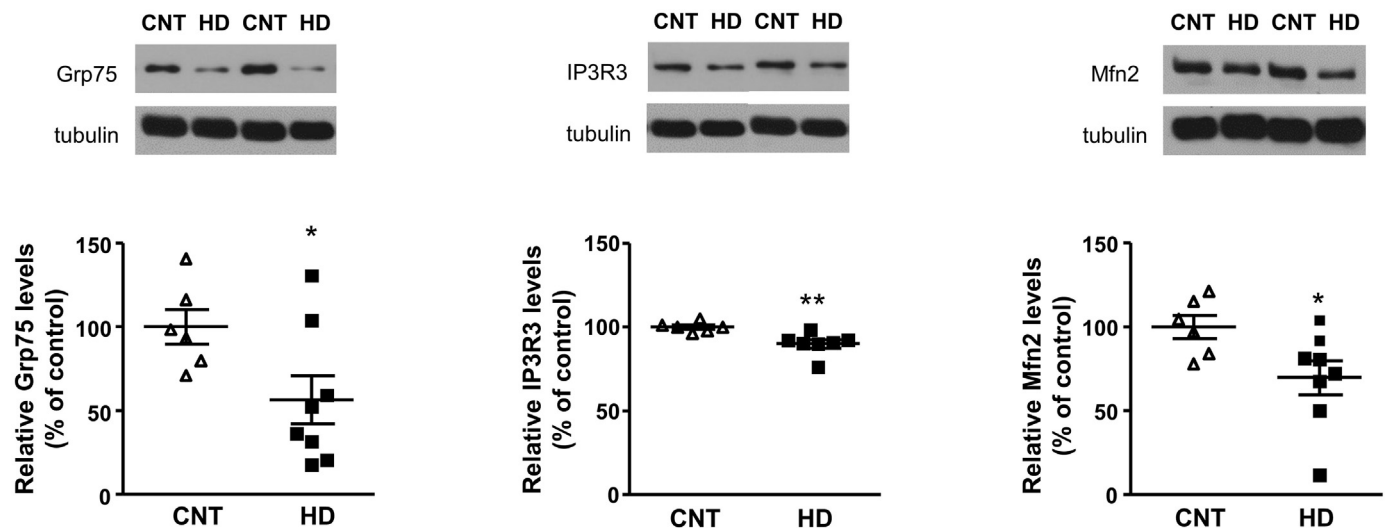
Fig. 5. Decrease of MAM proteins in the striatum of both R6/1 and $Hdh_{Q7/Q111}$ mutant mice. (A) Representative Western Blots showing the levels of Grp75, IP3R3, and Mfn2 in the striatum of WT and R6/1 mice at different disease stages (W, weeks; n=6-7 animals). α-tubulin was used as a loading control. Histograms show relative protein levels in R6/1 mice expressed as percentage of WT mice. Data represent mean ± SEM. *p < 0.05, ***p < 0.001 vs WT as determined by unpaired Student's t-test. (B) Representative Western Blots showing the levels of Grp75, IP3R3, and Mfn2 in the striatum of wild type HdhQ7/Q7 and mutant $Hdh_{Q7/Q111}$ mice at different disease stages (M, months; n= 6-7 animals). α-tubulin was used as a loading control. Histograms show relative protein levels in HdhQ7/Q111 mice expressed as percentage of WT mice. Data represent mean ± SEM. *p < 0.05 vs WT as determined by unpaired Student's t-test.

age, showing at 20 and 30 weeks a similar reduction. Finally, Mnf2 exhibited a small but significant decrease at the age of 20 weeks without significant differences at the other analyzed ages. Since reduction of MAMs proteins in R6/1 mice may come together with changes in ER protein levels, we next analyzed the protein expression of the ER chaperones calnexin and calreticulin, the ER Ca^{2+} sensor Stim1 and the structural ER protein Nogo (Fig. S4). Total and ER membrane fractions were obtained from WT and R6/1 at the age of 12 weeks and Western blot analysis performed. All analyzed proteins either in total (Fig. S4A) or ER fractions (Fig. S4B) showed similar levels between the two genotypes, suggesting no major ER protein alterations in R6/1 striatum.

Comparable data regarding MAMs protein levels were obtained when a different HD mouse model, the knock-in mutant $Hdh^{Q7/Q111}$ mice with a slow progression of the HD pathology (Wheeler et al., 1999), was analyzed (Fig. 5B). As in R6/1 mice, the striatal levels of Grp75 were found significantly decreased in $Hdh^{Q7/Q111}$ mutant mice compared with $Hdh^{Q7/Q7}$ wild type mice at 9 months of age, with a trend to decrease at 13 months and no significant differences at 18 months. For IP3R3, there was a sustained reduction beginning at 9 months of age while for Mfn2, a decrease only at 9 months was detected. Next, we investigated the levels of these MAMs proteins in postmortem brain tissue from the putamen of healthy and HD individuals (Fig. 6). Quantitative immunoblot analysis revealed a significant decrease of all analyzed proteins in the putamen of HD patients compared with controls (Grp75; control: 100 ± 10.36, HD: 56.48 ± 14.39; p = .0407, IP3R3; control: 100 ± 1253, HD: 89.91 ± 2535; p = .0062 and Mfn2; control: 100 ± 69.61, HD: 69.8 ± 10.07; p = .0407). Altogether, these results indicate that aberrant expression of MAMs proteins may contribute to disruption of ER-mitochondria contacts in HD mice striatum.

Our previous findings showing mitochondrial fission along with loss of ER-mitochondria contacts in R6/1 striatal cultures and altered expression of MAMs proteins in the striatum of HD mouse models and HD human brain may explain the specific vulnerability of this brain region to mutant huntingtin toxicity. To support this idea, we next analyzed MAMs proteins levels in the cortex (Fig. S5) and hippocampus (Fig. S6) of both R6/1 and $Hdh^{Q7/Q111}$ mutant mice as well as in HD human cortex (Fig. S7A) and hippocampus (Fig. S7B). Although, a significant

change for Grp75 levels was found in the cortex of 12 weeks-old R6/1 mice (Fig. S5A), no major changes were detected for protein (Grp75, IP3R3, Mfn2) nor for brain region (cortex and hippocampus) in HD versus WT or control samples, which underline the relevance of these changes in deregulating ER-mitochondria crosstalk particularly in the striatum.

3.6. Impaired ER-mitochondria Ca^{2+} transfer in R6/1 striatal cultures

Considering the observed reduction of ER and mitochondria contacts in R6/1 striatal cultures, we wondered whether Ca^{2+} exchange between these two compartments could also be altered and contribute to disruption of Ca^{2+} homeostasis. To this aim, the levels of intracellular Ca^{2+} (Cai^{2+}) and the mitochondrial membrane potential ($\Delta\Psi m$) were simultaneously monitored using Fluo4 and TMRM, respectively. No differences between genotypes in basal Cai^{2+} and $\Delta\Psi m$ were observed (Fig. 7A). Next, Ca^{2+} release from the ER was induced by using thapsigargin (TG), which depletes ER Ca^{2+} stores inhibiting sarco-endoplasmic reticulum Ca^{2+}-ATPase (SERCA) activity. We found that TG treatment induced a higher increase in Cai^{2+} concentration in R6/1 striatal neurons than in WT neurons (~ 50% increase; p < .05; Fig. 7B). This phenomenon could be due to reduced mitochondria Ca^{2+} uptake by R6/1 neurons, since the robust increase in Cai^{2+} was associated with a slighter depolarization of the $\Delta\Psi m$ compared to WT neurons (~ 20% less decrease; p < .05; Fig. 7B) as indicated by TMRM fluorescence. Next, to demonstrate that R6/1 striatal neurons exhibit mitochondria Ca^{2+} uptake deficits, primary neuronal cultures were treated with FCCP, an uncoupler of oxidative phosphorylation that collapses the mitochondrial membrane potential, to induce a maximal depolarization. According to our hypothesis, the increase on Cai^{2+} induced by FCCP-mediated mitochondrial depolarization was lower in R6/1 neurons compared to WT neurons (~ 25% less increase; p < .001; Fig. 7C) as well as the depolarization of the $\Delta\Psi m$ (~ 25% less decrease; p < .001; Fig. 7C). Representative traces of individual cells are shown in Fig. 7D.

Overall, these results suggest that the reduction on mitochondrial Ca^{2+} retention could be due to altered ER-mitochondrial Ca^{2+} transfer and therefore with disturbances in ER-mitochondria contacts. In agreement with this hypothesis, treatment of R6/1 neurons with Mdivi-
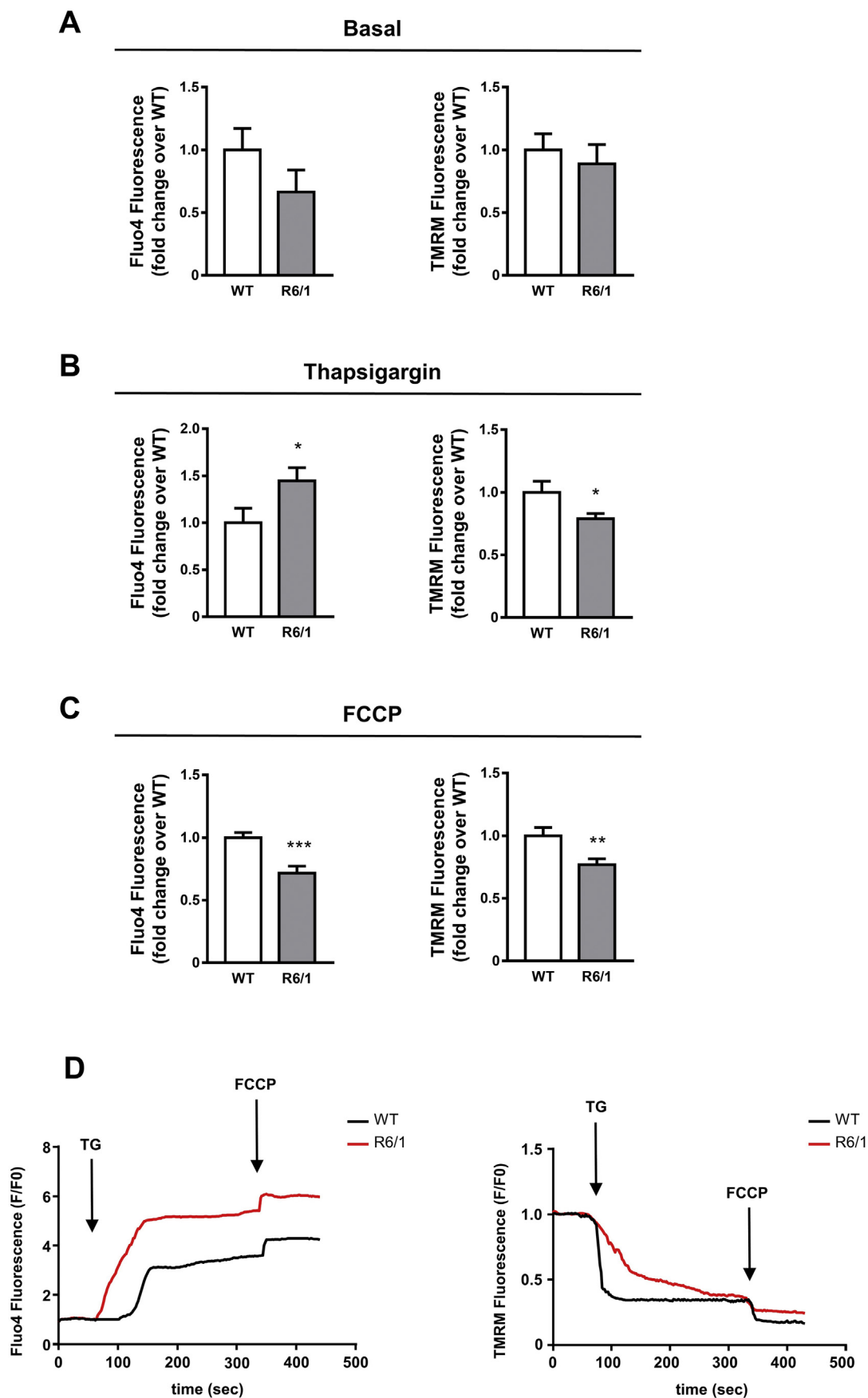
Fig. 6. MAM proteins are also reduced in putamen postmortem samples from HD patients. Representative Western Blots showing the levels of Grp75, IP3R3 and Mfn2 in post-mortem putamen samples from control (n = 6) and HD patients (n = 8). α-tubulin was used as a loading control. Histograms show relative protein levels in HD samples expressed as percentage of control samples. Data represent mean ± SEM. *p < 0.05, **p < 0.01 vs control as determined by unpaired Student's t-test

A

Basal

B

Thapsigargin

C

FCCP

D
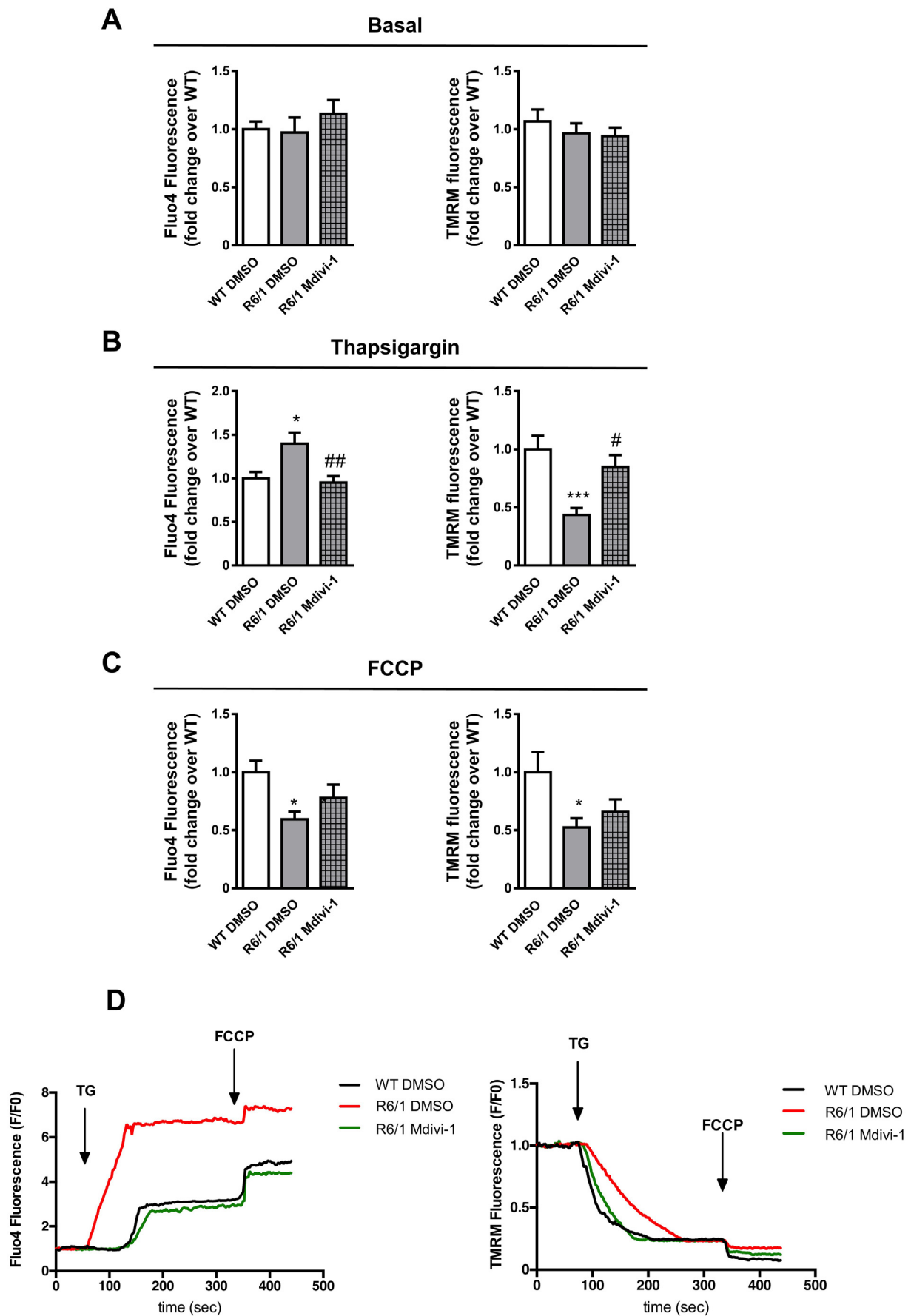
(caption on next page)

Fig. 7. ER-mitochondrial Ca^{2+} transfer is altered in R6/1 primary striatal neurons. Primary striatal neurons loaded with Fluo4 (5 μM) and TMRM (20 nM) were stimulated with TG (0.5 μM) and FCCP (2 μM). Bar histograms showing fluorescence folds change of Fluo4 or TMRM at basal conditions (A) and after thapsigargin (B) or FCCP (C) exposure. (D) Representative Fluo4 and TMRM fluorescence traces from WT (black) and R6/1 (red) individual striatal neurons following thapsigargin (TG) and FCCP stimulation. For single-cell imaging studies, data represent mean ± SEM of 6 independent experiments. *p < 0.05, **p < 0.01, ***p < 0.001 vs WT as determined by unpaired Student's t-test. (For interpretation of the references to colour in this figure legend, the reader is referred to the web version of this article.)

1 prevented the increase in Ca_i^{2+} levels and the decrease in mitochondrial membrane potential following TG incubation (Fig. 8B). Similarly, mitochondria Ca^{2+} uptake disturbances, manifested as reduced Ca_i^{2+} concentration and TMRM fluorescence in depolarized FCCP conditions, were also ameliorated in R6/1-treated Mdivi-1 neurons (Fig. 8C). Notice that Mdivi-1 treatment did not alter Basal Fluo4 or TMRM fluorescence (Fig. 8A). Altogether, these findings support the view that altered ER-mitochondria tethering underlies Ca^{2+} homeostasis defects in HD striatum.

4. Discussion

Disruption of mitochondrial function and calcium (Ca^{2+}) homeostasis are well-recognized pathological features of HD that contribute to the preferential degeneration of the striatum in this disorder (Browne, 2008; Lezi and Swerdlow, 2012). However, little is known on how changes in mitochondria dynamics induced by mutant huntingtin may affect Ca^{2+} mitochondrial handling and mitochondrial oxidative stress. In this study, we provide evidence showing that deregulation of mitochondrial fission events may have a detrimental role in HD striatal pathology by (1) enacting loss of ER-mitochondria contacts with the consequent disturbances in intracellular Ca^{2+} homeostasis and (2) favoring mitochondrial production of superoxide.

Mitochondrial dynamics is a crucial event that determines mitochondrial morphology and size but also regulates mitochondrial distribution and function (Chan, 2006). Previous results from our laboratory and others have reported that this process is disrupted in several HD cellular and mouse models revealing increased mitochondrial fragmentation and therefore an imbalance towards mitochondrial fission events (Reddy, 2014; Cherubini et al., 2015; Guo et al., 2013). In line with this evidence, in this study we have shown impaired mitochondrial dynamics, evidenced by a prominent mitochondrial fragmentation and disruption of the mitochondrial network in the striatum but not in the cortex or hippocampus of exon-1 R6/1 transgenic mice. This excessive mitochondrial fission was Drp1-dependent since pre-treatment with Mdvi-1, a well-known inhibitor of mitochondrial fission that blocks GTPase Drp1 activity (Cassidy-Stone et al., 2008) completely restored mitochondrial shape and network parameters. Indeed and according with aberrant Drp1 activity, a trend increase tendency in Drp1 tetrameric protein forms and Drp1 mRNA levels was found in R6/1 striatal primary cultures when compared with WT cultures. These findings are in agreement with previous studies from our group and others showing increased Drp1 activity in HD striatal neurons as well as a protective effect of Mdvi-1 against mutant huntingtin induced striatal neuropathology (Cherubini et al., 2015; Shirendeb et al., 2011; Manczak and Hemachandra Reddy, 2015).

The increase in mitochondrial fragmentation that we have reported in HD striatum, could negatively interferes with neuronal function at different levels. First, inhibition of mitochondrial fusion has been associated with impaired Oxidative Phosphorylation (OXPHOS) and ROS production in different cellular types (Liesa and Shirihai, 2013) stressing the idea that mitochondrial function is strongly dependent on preserved mitochondria structure. Accordingly, we have observed that the increase in mitochondria superoxide production in R6/1 striatal cultures can be reversed after normalization of the mitochondria network by Mdvi-1 treatment. Similarly, Manzcak and colleagues have described a beneficial effect of Mdvi-1 in reducing mitochondrial fission, OXPHOS activity and free radicals generation in HD cellular models (Manczak and Hemachandra Reddy, 2015). Second, the

propensity of mitochondria to undergo fragmentation in HD striatum could result in the disruption of ER-mitochondria contacts negatively acting on the role of mitochondria in Ca^{2+} buffering. According with this idea, we found in R6/1 striatal neurons an important decrease in ER-mitochondrial apposition evidenced by a loss of co-localization between both organelles. Again, restoration of the mitochondrial network by Mdvi-1 reversed the loss of ER-mitochondria contacts, supporting the idea that increased mitochondrial fission is critically involved in the disruption of ER-mitochondria tethering in HD striatum. Similarly, parkin dysfunction in Parkinson's disease (PD) models has been associated with altered mitochondrial fragmentation and defective ER-mitochondria contacts with the subsequent alteration in mitochondrial Ca^{2+} uptake (Calì et al., 2013a; Zheng et al., 2017; Celardo et al., 2016). Likewise, reduction of PINK1 expression in human dopaminergic neuroblastoma cells, impairs mitochondria fusion and mitochondria motility altering ER-mitochondria association (Parrado-Fernández et al., 2018).

Nevertheless, besides the disruption of the mitochondrial network other mechanisms could be involved in the reduction of ER-mitochondria contacts in HD striatum. MAMs contain specific proteins that facilitate the physical association between the ER and mitochondria. Therefore, alteration in the expression of MAM-resident proteins may also contribute to aberrant ER-mitochondria communication. Supporting this hypothesis, we found in the striatum but not in the cortex or hippocampus of two different HD mouse models and in human HD striatum a significant reduction in ER-anchored IP3 receptor 3 and in chaperone Grp75 protein levels. A decrease in mitofusin-2 was only observed in HD human putamen. The fact that the reduction of MAM's proteins in striata of HD mouse models runs in parallel to the behavioral disturbances, points at ER-mitochondria loss of contacts as a critical contributor rather than a primary cause of striatal vulnerability. Nevertheless, the decrease in MAMs proteins can be detected at early-middle disease stages suggesting that this reduction is not just a consequence of striatal dysfunction but a factor in HD progression. Perturbations in several proteins of the ER-mitochondria interface have also been reported in other neurodegenerative disorders either enhancing or decreasing ER-mitochondria juxtaposition. Thus, up-regulation of several MAM-associated proteins along with increased function of MAM and ER-mitochondria interaction has been observed both in Alzheimer's disease (AD) murine models and in AD human fibroblasts (Area-Gomez et al., 2012; Hedskog et al., 2013). In contrast, different Amyotrophic lateral sclerosis or PD-causing mutations have been associated with either higher or lower ER-mitochondria contacts by altering expression or binding between MAM-resident proteins (Erpapazoglou et al., 2017).

So far, these findings suggest that direct communication between mitochondria and ER is compromised in HD. Given that a major function of ER-mitochondria contacts is to transfer Ca^{2+} from ER stores to mitochondria (Rizzuto et al., 1998) and given the reported mitochondrial Ca^{2+} mishandling in HD pathology (Milakovic et al., 2006; Rosenstock et al., 2010; Naia et al., 2017), we hypothesize that disruption of ER-mitochondria tethering will contribute to Ca^{2+} dishomeostasis in HD striatum. In agreement with this hypothesis, we demonstrated in HD striatal neurons that induction of Ca^{2+} release from the ER produces an immediate increase in intracellular Ca^{2+} (Ca_i^{2+}) associated with a low mitochondrial depolarization, which is suggestive of defective mitochondrial Ca^{2+} uptake. These results prompted us to propose a new but not exclusive mechanism for mitochondrial Ca^{2+} mishandling in HD, which differs from some studies previously reported
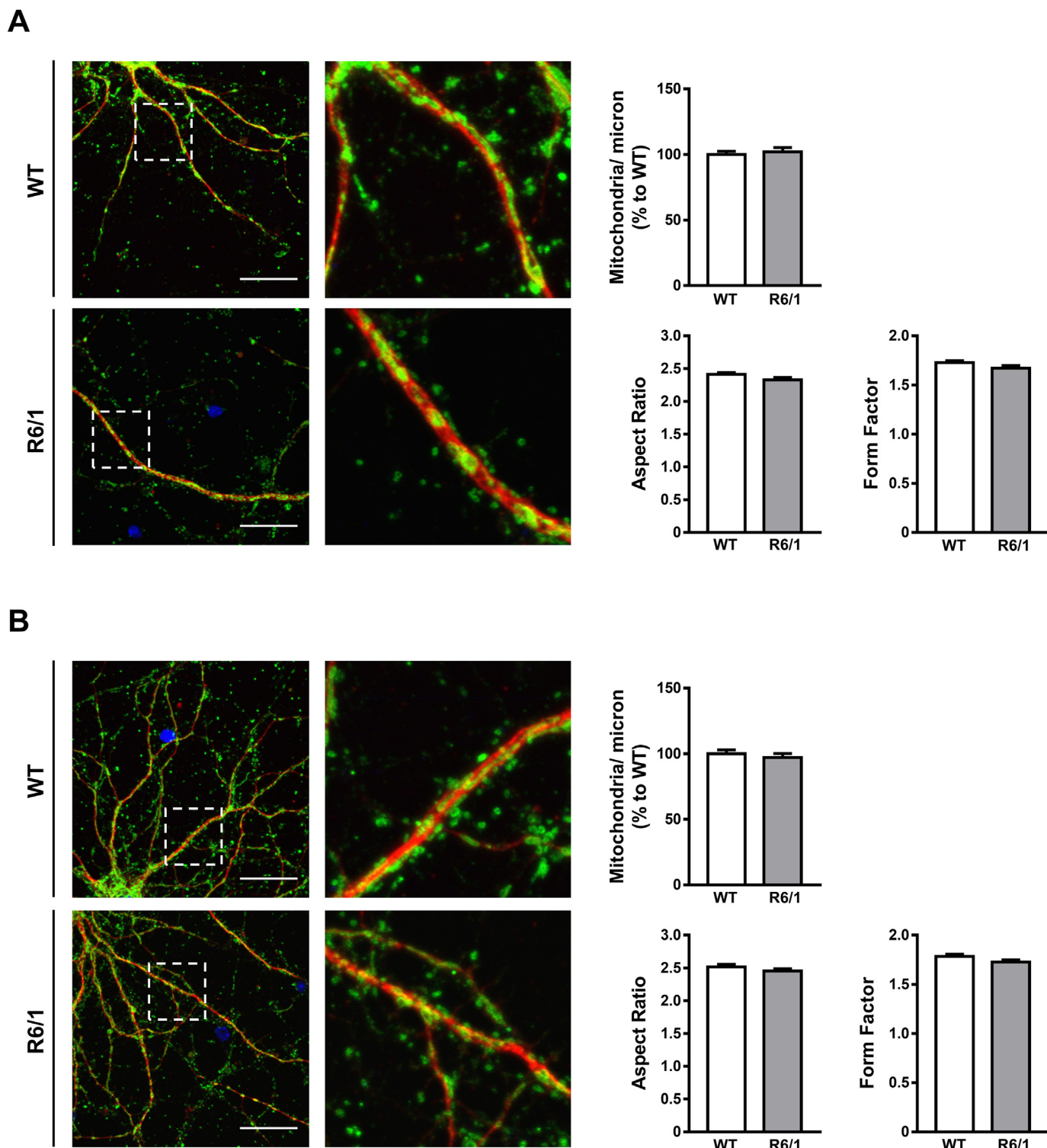
A

B

Fig. 8. Mdivi-1 treatment restores ER-mitochondrial Ca^{2+} transfer in R6/1 primary striatal neurons. Primary striatal neurons treated with vehicle (DMSO) or Mdivi-1 (25 μM) and successively loaded with Fluo4 (5 μM) and TMRM (20 nM) were stimulated with TG (0.5 μM) and FCCP (2 μM). Bar histograms showing fluorescence folds change of Fluo4 or TMRM at basal conditions (A) and after thapsigargin (B) or FCCP (C) exposure. (D) Representative Fluo4 and TMRM fluorescence traces from WT (black), R6/1 (red) and Mdivi-1-treated R6/1 (green) individual striatal neurons following thapsigargin (TG) and FCCP stimulation. For single-cell imaging studies, data represent mean ± SEM of 3 independent experiments. *p < 0.05, ***p < 0.001 vs WT and #p < 0.05, ##p < 0.01 vs vehicle-treated R6/1 as determined by One-way ANOVA analysis with Tukey's multiple comparison test.

(Milakovic et al., 2006; Choo et al., 2004). These studies attribute the aberrant increase in Ca$_i^{2+}$ to the enhanced mitochondrial sensitivity to Ca^{2+} loads. However, the recovery of the mitochondrial Ca^{2+} capacity and the inhibition of mitochondrial permeability transition pore (PTP)

induction failed to ameliorate either the behavioral or the neuropathological features of the disease (Perry et al., 2010). Other studies have reported an age-dependent increase in the Ca^{2+} loading capacity of striatal mitochondria (Brustovetsky et al., 2005) or even no changes

(Oliveira et al., 2007). These discrepancies may be the result of differences in the analyzed disease stage or the use of isolated mitochondria versus intact striatal neurons. Our results obtained in an appropriate neuronal context, that is HD-derived striatal neurons, suggest that Ca^{2+} dishomeostasis in HD could depend not only on intrinsic mitochondrial Ca^{2+} buffering capacity but also on MAMs integrity. Supporting this view, treatment of R6/1 mutant huntingtin striatal neurons with the Drp1 inhibitor Mdivi-1, not only restored the loss of ER-mitochondria contacts but also the ER-mitochondria Ca^{2+} transfer improving Ca^{2+} homeostasis defects. Indeed, compelling evidence have highlighted the importance of a proper distance between the ER and mitochondria to transfer Ca^{2+} efficiently between these two organelles (Csordás et al., 2010; Shin and Muallem, 2010). Thus, the gap between ER and mitochondria generated by aberrant mitochondrial fragmentation, could be sufficient to isolate mitochondria from the ER-Ca^{2+} leakage, impeding properly mitochondrial Ca^{2+} handling in HD striatum.

5. Conclusion

In sum, considering the critical role played by mitochondrial Ca^{2+} in the modulation of numerous physiological responses, particularly in neurons (Brini et al., 2014), the disruption of ER-mitochondria tethers in the HD striatum by either increased mitochondria fission or loss of MAM-resident proteins could play a pivotal role on Ca^{2+} dishomeostasis and contribute to striatal dysfunction and degeneration in HD.

Supplementary data to this article can be found online at https://doi.org/10.1016/j.nbd.2020.104741.

Declaration of competing interest

None

Authors' contribution

M.C, L.L-M and S.G conceived and designed the experiments. M.C performed biochemical studies and calcium assay. L.L-M performed immunocytochemistry and confocal microscopy image analysis, biochemical studies and PLA assays. S.G wrote the paper. All authors read and approved the final manuscript.

References

Ahmad, T., Aggarwal, K., Pattnaik, B., Mukherjee, S., Sethi, T., Tiwari, B.K., et al., 2013. Computational classification of mitochondrial shapes reflects stress and redox state. Cell Death Dis. 4 e461-10.

Anglada-Huguet, M., Giralt, A., Rué, L., Alberch, J., Xifró, X., 2016. Loss of striatal 90-kDa ribosomal S6 kinase (Rsk) is a key factor for motor, synaptic and transcription dysfunction in Huntington's disease. Biochim. Biophys. Acta Mol. basis Dis. 1862, 1255–1266.

Area-Gomez, E., Del Carmen Lara Castillo, M., Tambini, M.D., Guardia-Laguarta, C., AJC, D.G., Madra, M., et al., 2012. Upregulated function of mitochondria-associated ER membranes in Alzheimer disease. EMBO J. 31, 4106–4123.

Bozidis, P., Williamson, C.D., Colberg-Poley, A.M., 2007. Isolation of endoplasmic reticulum, mitochondria, and mitochondria-associated membrane fractions from transfected cells and from human cytomegalovirus-infected primary fibroblasts. Curr. Protoc. Cell Biol. 37, 3.27.1–3.27.23.

Brini, M., Calì, T., Ottolini, D., Carafoli, E., 2014. Neuronal calcium signaling: function and dysfunction. Cell. Mol. Life Sci. 71, 2787–2814.

Browne, S.E., 2008. Mitochondria and Huntington's disease pathogenesis: insight from genetic and chemical models. Ann. N. Y. Acad. Sci. 1147, 358–382.

Brustovetsky, N., LaFrance, R., Purl, K.J., Brustovetsky, T., Keene, C.D., Low, W.C., et al., 2005. Age-dependent changes in the calcium sensitivity of striatal mitochondria in mouse models of Huntington's disease. J. Neurochem. 93, 1361–1370.

Calì, T., Ottolini, D., Brini, M., 2013a. Calcium and endoplasmic reticulum-mitochondria tethering in Neurodegeneration. DNA Cell Biol. 32, 140–146.

Calì, T., Ottolini, D., Negro, A., Brini, M., 2013b. Enhanced parkin levels favor ER-mitochondria crosstalk and guarantee Ca2+ transfer to sustain cell bioenergetics. Biochim. Biophys. Acta Mol. basis Dis. 1832, 495–508.

Campello, S., Scorrano, L., 2010. Mitochondrial shape changes: orchestrating cell pathophysiology. EMBO Rep. 11, 678–684.

Cassidy-Stone, A., Chipuk, J.E., Ingerman, E., Song, C., Yoo, C., Kuwana, T., et al., 2008. Chemical inhibition of the mitochondrial division dynamin reveals its role in Bax/Bak-dependent mitochondrial outer membrane permeabilization. Dev. Cell 14, 193–204.

Celardo, I., Costa, A.C., Lehmann, S., Jones, C., Wood, N., Mencacci, N.E., et al., 2016. Mitofusin-mediated ER stress triggers neurodegeneration in pink1/parkin models of Parkinson's disease. Cell Death Dis. 7, e2271.

Chan, D.C., 2006. Mitochondrial fusion and fission in mammals. Annu. Rev. Cell Dev. Biol. 22, 79–99.

Cherubini, M., Puigdellívol, M., Alberch, J., Ginés, S., 2015. Cdk5-mediated mitochondrial fission: a key player in dopaminergic toxicity in Huntington's disease. Biochim. Biophys. Acta Mol. basis Dis. 1852, 2145–2160.

Cho, B., Kim, H., Cho, H.M., Kim, H.J., Jeong, J., Park, S.K., et al., 2014. CDK5-dependent inhibitory phosphorylation of Drp1 during neuronal maturation. Exp. Mol. Med. 46, 1–10.

Choo, Y.S., Johnson, G.V.W., MacDonald, M., Detloff, P.J., Lesort, M., 2004. Mutant huntingtin directly increases susceptibility of mitochondria to the calcium-induced permeability transition and cytochrome c release. Hum. Mol. Genet. 13, 1407–1420.

Costa, V., Giacomello, M., Hudec, R., Lopreiato, R., Ermak, G., Lim, D., et al., 2010. Mitochondrial fission and cristae disruption increase the response of cell models of Huntington's disease to apoptotic stimuli. EMBO Mol. Med. 2, 490–503.

Csordás, G., Renken, C., Várnai, P., Walter, L., Weaver, D., Buttle, K.F., et al., 2006. Structural and functional features and significance of the physical linkage between ER and mitochondria. J. Cell Biol. 174, 915–921.

Csordás, G., Várnai, P., Golenár, T., Roy, S., Purkins, G., Schneider, T.G., et al., 2010. Imaging interorganelle contacts and local calcium dynamics at the ER-mitochondrial interface. Mol. Cell 39, 121–132.

De Brito, O.M., Scorrano, L., 2008. Mitofusin 2 tethers endoplasmic reticulum to mitochondria. Nature. 456, 605–610.

Erpapazoglou, Z., Mouton-Liger, F., Corti, O., 2017. From dysfunctional endoplasmic reticulum-mitochondria coupling to neurodegeneration. Neurochem. Int. 109, 171–183.

Frederick, R.L., Shaw, J.M., 2007. Moving mitochondria: establishing distribution of an essential organelle. Traffic. 8, 1668–1675.

Giacomello, M., Hudec, R., Lopreiato, R., 2011. Huntington's disease, calcium, and mitochondria. BioFactors. 37, 206–218.

Guo, X., Mochly-rosen, D., Qi, X., Guo, X., Disatnik, M., Monbureau, M., et al., 2013. Inhibition of mitochondrial fragmentation diminishes Huntington's disease – associated neurodegeneration. J. Clin. Invest. 123, 5371–5388.

Hedskog, L., Pinho, C.M., Filadi, R., Ronnback, A., Hertwig, L., Wiehager, B., et al., 2013. Modulation of the endoplasmic reticulum-mitochondria interface in Alzheimer's disease and related models. Proc. Natl. Acad. Sci. 110, 7916–7921.

Huntington, G., 1872. On chorea. Med. Surg. Rep. A Wkly J. 26, 317–321.

Iwasawa, R., Mahul-Mellier, A.L., Datler, C., Pazarentzos, E., Grimm, S., 2011. Fis1 and Bap31 bridge the mitochondria-ER interface to establish a platform for apoptosis induction. EMBO J. 30, 556–568.

Koopman, W.J.H., Visch, H.J., Smeitink, J.A.M., Willems, P.H.G.M., 2006. Simultaneous quantitative measurement and automated analysis of mitochondrial morphology, mass, potential, and motility in living human skin fibroblasts. Cytom Part A. 69, 1–12.

Lezi, E., Swerdlow, R.C., 2012. Advances in mitochondrial medicine. J. Inborn Errors Metab. Screen. 942, 269–286.

Liesa, M., Shirihai, O.S., 2013. Mitochondrial dynamics in the regulation of nutrient utilization and energy expenditure. Cell Metab. 17, 491–506.

Manczak, M., Hemachandra Reddy, P., 2015. Mitochondrial division inhibitor 1 protects against mutant huntingtin-induced abnormal mitochondrial dynamics and neuronal damage in Huntington's disease. Hum. Mol. Genet. 24, 7308–7325.

Mendes, C.C.P., Gomes, D.A., Thompson, M., Souto, N.C., Goes, T.S., Goes, A.M., et al., 2005. The type III inositol 1,4,5-trisphosphate receptor preferentially transmits apoptotic Ca2+ signals into mitochondria. J. Biol. Chem. 280, 40892–40900.

Milakovic, T., Quintanilla, R.A., Johnson, G.V.W., 2006. Mutant Huntingtin expression induces mitochondrial calcium handling defects in clonal striatal cells: functional consequences. J. Biol. Chem. 281, 34785–34795.

Møllersen, L., Rowe, A.D., Larsen, E., Rognes, T., Klungland, A., 2010. Continuous and periodic expansion of CAG repeats in huntington's disease R6/1 mice. PLoS Genet. 6, 1–11.

Morton, A.J., Glynn, D., Leavens, W., Zheng, Z., Faull, R.L.M., Skepper, J.N., et al., 2009. Paradoxical delay in the onset of disease caused by super-long CAG repeat expansions

in R6/2 mice. Neurobiol. Dis. 33, 331–341.

Naia, L., Ferreira, I.L., Ferreiro, E., Rego, A.C., 2017. Mitochondrial Ca2 + handling in Huntington's and Alzheimer's diseases – role of ER-mitochondria crosstalk. Biochem. Biophys. Res. Commun. 483, 1069–1077.

Nakamura, T., Shiu, A.D., Haun, F., Cho, D., Holland, E.A., La, S.A.R., et al., 2013. Mutant huntingtin-induced mitochondrial fragmentation. Antioxid. Redox Signal. 19, 1173–1184.

Oliveira, J.M.A., Jekabsons, M.B., Chen, S., Lin, A., Rego, A.C., Gonçalves, J., et al., 2007. Mitochondrial dysfunction in Huntington's disease: the bioenergetics of isolated and in situ mitochondria from transgenic mice. J. Neurochem. 101, 241–249.

Orr, A.L., Li, S., Wang, C.-E., Li, H., Wang, J., Rong, J., et al., 2008. N-terminal mutant huntingtin associates with mitochondria and impairs mitochondrial trafficking. J. Neurosci. 28, 2783–2792.

Ottolini, D., Calì, T., Negro, A., Brini, M., 2013. The Parkinson disease-related protein DJ-1 counteracts mitochondrial impairment induced by the tumour suppressor protein p53 by enhancing endoplasmic reticulum-mitochondria tethering. Hum. Mol. Genet. 22, 2152–2168.

Panov, A.V., Gutekunst, C.A., Leavitt, B.R., Hayden, M.R., Burke, J.R., Strittmatter, W.J., et al., 2002. Early mitochondrial calcium defects in Huntington's disease are a direct effect of polyglutamines. Nat. Neurosci. 5, 731–736.

Parrado-Fernández, C., Schneider, B., Ankarcrona, M., Conti, M.M., Cookson, M.R., Kivipelto, M., et al., 2018. Reduction of PINK1 or DJ-1 impair mitochondrial motility in neurites and alter ER-mitochondria contacts. J. Cell. Mol. Med. 22, 5439–5449.

Perry, G.M., Tallaksen-Greene, S., Kumar, A., Heng, M.Y., Kneynsberg, A., van Groen, T., et al., 2010. Mitochondrial calcium uptake capacity as a therapeutic target in the R6/2 mouse model of Huntington's disease. Hum. Mol. Genet. 19, 3354–3371.

Raturi, A., Simmen, T., 2013. Where the endoplasmic reticulum and the mitochondrion tie the knot: the mitochondria-associated membrane (MAM). Biochim. Biophys. Acta, Mol. Cell Res. 1833, 213–224.

Reddy, P.H., 2014. Increased mitochondrial fission and neuronal dysfunction in Huntington's disease: implications for molecular inhibitors of excessive mitochondrial fission. Drug Discov. Today 19, 951–955.

Rizzuto, R., Pinton, P., Carrington, W., Fay, F.S., Fogarty, K.E., Lifshitz, L.M., et al., 1998. Close contacts with the endoplasmic reticulum as determinants of close contacts with the endoplasmic reticulum as determinants of mitochondrial Ca 2+ responses. Science (80-). 280, 1763–1766.

Rosenstock, T.R., Bertoncini, C.R.A., Teles, A.V., Hirata, H., Fernandes, M.J.S., Smaili, S.S., 2010. Glutamate-induced alterations in Ca2 + signaling are modulated by mitochondrial Ca2 + handling capacity in brain slices of R6/1 transgenic mice. Eur. J. Neurosci. 32, 60–70.

Ross, C.A., Margolis, R.L., 2001. Huntington ' s disease. Clin. Neurosci. Res. 1, 142–152.

Rowland, A.A., Voeltz, G.K., 2012. Endoplasmic reticulum-mitochondria contacts: function of the junction. Nat. Rev. Mol. Cell Biol. 13, 607–615.

Rusiñol, A.E., Cui, Z., Chen, M.H., Vance, J.E., 1994. A unique mitochondria-associated membrane fraction from rat liver has a high capacity for lipid synthesis and contains pre-Golgi secretory proteins including nascent lipoproteins. J. Biol. Chem. 269, 27494–27502.

Shin, D.M., Muallem, S., 2010. What the mitochondria see. Mol. Cell 39, 6–7.

Shirendeb, U., Reddy, A.P., Manczak, M., Calkins, M.J., Mao, P., Tagle, D.A., et al., 2011. Abnormal mitochondrial dynamics, mitochondrial loss and mutant huntingtin oligomers in Huntington's disease: implications for selective neuronal damage. Hum. Mol. Genet. 20, 1438–1455.

Shirendeb, U.P., Calkins, M.J., Manczak, M., Anekonda, V., Dufour, B., McBride, J.L., et al., 2012. Mutant Huntingtin's interaction with mitochondrial protein Drp1 impairs mitochondrial biogenesis and causes defective axonal transport and synaptic degeneration in Huntington's disease. Hum. Mol. Genet. 21, 406–420.

Song, W., Chen, J., Petrilli, A., Liot, G., Klinglmayr, E., Zhou, Y., et al., 2011. Mutant huntingtin binds the mitochondrial fission GTPase dynamin-related protein-1 and increases its enzymatic activity. Nat Med. 17, 377–383.

Stoica, R., De Vos, K.J., Paillusson, S., Mueller, S., Sancho, R.M., Lau, K.F., et al., 2014. ER-mitochondria associations are regulated by the VAPB-PTPIP51 interaction and are disrupted by ALS/FTD-associated TDP-43. Nat. Commun. 5.

Szabadkai, G., Simoni, A.M., Bianchi, K., De Stefani, D., Leo, S., Wieckowski, M.R., et al., 2006. Mitochondrial dynamics and Ca2 + signaling. Biochim. Biophys. Acta, Mol. Cell Res. 1763, 442–449.

Vonsattel, J.P.G., DiFiglia, M., 1998. Huntington disease. J. Neuropathol. Exp. Neurol. 57, 369–384.

Vonsattel, J.P., Myers, R.H., Stevens, T.J., Ferrante, R.J., Bird, E.D., Richardson, E.P.J., 1985. Neuropathological classification of Huntington's disease. J. Neuropathol. Exp. Neurol. 44, 559–577.

Wheeler, V.C., Auerbach, W., White, J.K., Srinidhi, J., Auerbach, A., Ryan, A., et al., 1999. Length-dependent gametic CAG repeat instability in the Huntington's disease knock-in mouse. Hum. Mol. Genet. 8, 115–122.

Zheng, Q., Jiang, Y., Zhang, A., Cui, L., Xia, L., Luo, M., 2017. The mechanism of mitochondria-mediated pathway in the apoptosis of platelets in immune-induced bone marrow failure. Chin. J. Phys. 60, 338–344.

Zhu, P.P., Patterson, A., Stadler, J., Seeburg, D.P., Sheng, M., Blackstone, C., 2004. Intra- and intermolecular domain interactions of the C-terminal GTPase effector domain of the multimeric dynamin-like GTPase Drp1. J. Biol. Chem. 279, 35967–35974.